Eur. Phys. J. E **8**, 437–443 (2002)
DOI 10.1140/epje/i2002-10032-2

THE EUROPEAN PHYSICAL JOURNAL E
EDP Sciences

Roughness and dynamics of a contact line of a viscous fluid on a disordered substrate

S. Moulinet[a], C. Guthmann, and E. Rolley

Laboratoire de Physique Statistique de l'Ecole Nomale Supérieure associé au CNRS et aux Universités Paris 6 et Paris 7, 24 rue Lhomond, 75231 Paris Cedex 05, France

Received 18 April 2002

Abstract. We have studied the roughness and the dynamics of the contact line of a viscous liquid on a disordered substrate. We have used photolithographic techniques to obtain a controlled disorder with a correlation length $\xi = 10\,\mu$m. Liquids with different viscosity were used: water and aqueous glycerol solution. We have found that the roughness W of the contact line depends neither on the viscosity nor on the velocity v of the contact line for v in the range 0.2–20 μm/s. W is found to scale with the length L of the line as L^ζ with a roughness exponent $\zeta = 0.51 \pm 0.03$. This value is similar to the one obtained with superfluid helium. In the present experiment, we have checked that the motion of the contact line is actually overdamped, so that the phenomenological equation first proposed by Ertas and Kardar should be relevant. However, our measurement of ζ is in disagreement with the predicted value $\zeta = 0.39$. We have also analyzed the avalanche-like motion of the contact line. We find that the size distribution does not follow a power law dependence.

PACS. 46.65.+g Random phenomena and media – 64.60.Ht Dynamic critical phenomena

1 Introduction

Recently, many works have been devoted to understand the dynamics and the shape of elastic systems in random media. Examples of such systems are domains walls in ferromagnets [1], charge density waves [2]. In this article we are interested in the motion of a contact line on a heterogenous solid substrate.

In a partial wetting situation, the meniscus meets the solid surface along the contact line (CL), which is the boundary between the dry and the wet part of the substrate. On a disordered surface, the shape of the CL (Fig. 1) is distorted as a result of the competition between its stiffness and the defects of the substrate. It has been proposed by Ertas and Kardar [3] that the motion of the CL can be described by the following phenomenological equation:

$$\mu\left(v + \frac{\partial \eta(x,t)}{\partial t}\right) = F_{\rm ext} + f(x, vt + \eta(x,t)) + \mathcal{K}[\eta]\,, \quad (1)$$

where $\eta(x,t)$ is the displacement of the line with respect to its average position vt, μ is a dissipative coefficient, $f(x,y)$ is the random force due to the disorder of the substrate, and $\mathcal{K}[\eta]$ is an elastic restoring force. The distortion of the meniscus is responsible for the long-ranged elastic interaction, as pointed out by Joanny and de Gennes [4]:

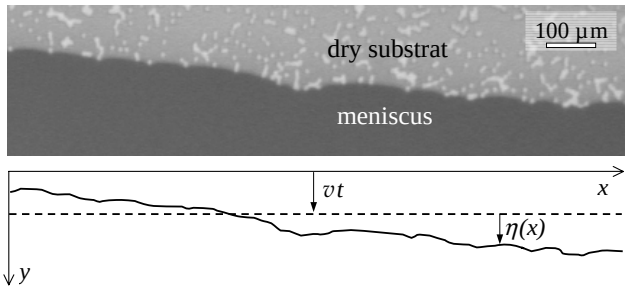

Fig. 1. Upper part: image of the contact line obtained with an ordinary CCD camera. Lower part: the position $\eta(x,t) \equiv y(x,t) - vt$ of the CL is defined with respect to its average position vt.

$$\mathcal{K}[\eta] = -\frac{1}{\pi}\gamma \sin^2\theta \int \mathrm{d}x' \frac{\eta(x',t)}{(x-x')^2}\,, \quad (2)$$

where the summation is taken over the whole CL, γ is the liquid-vapor surface tension and θ is the angle under which the meniscus meets the substrate (contact angle).

The fluctuations of the CL around its average position are characterized by the scaling behaviour of its roughness W defined by: $W(L) = \left\langle\left\langle(\eta(L+x_0) - \eta(x_0))^2\right\rangle\right\rangle^{1/2}$ (the average is taken over x_0 along the line and over successive configurations of the CL). One expects W to vary with the scale L as L^ζ, where ζ is called the roughness exponent. At equilibrium, for a small-amplitude disorder, equation (1)

[a] e-mail: moulinet@lps.ens.fr

has been solved by several techniques, and the common prediction is $\zeta = 1/3$ [5,3]. This has been confirmed experimentally [6]. What happens at depinning threshold is still controversial. Following Narayan and Fisher [2], Ertas and Kardar have argued that the result at equilibrium should hold at the threshold. However, it was shown recently by Chauve *et al.* that extending Ertas' functional renormalisation group calculation up to two-loop order leads to a value of ζ larger than 1/3 [7]. This result is consistent with a precise numerical calculation by Rosso and Krauth, which yields $\zeta = 0.388 \pm 0.002$ [8]. Numerical simulations of equation (1) have also been performed; Tanguy *et al.* found ($\zeta = 0.35 \pm 0.02$) [9], while Zhou *et al.* found ($\zeta \simeq 0.39$) [10]. Let us stress that all predicted values lie in the range 0.33–0.39.

Experiments have already been performed in our group [11]. Using superfluid helium on a rough substrate covered with cesium, the value of the roughness exponent was found to be $\zeta \simeq 0.55$. For this peculiar system, it was shown that the motion of the CL is not quasi-static: during a jump of the CL, the lateral depinning velocity is comparable to the velocity of capillary wave. As proposed by Schwarz and Fisher in the context of crack fronts [12], this may lead to dynamic stress overshoots and could explain the unexpectedly high value of ζ.

In order to test this hypothesis, and to study the behaviour of an ordinary overdamped system, it is necessary to use ordinary viscous liquids. Some results on the dynamics and structure of the CL have been obtained by Di Meglio [13] and Decker and Garoff [14]. However, in these experiments, the disorder could not be completely controlled. Thus we decided to transpose the helium/cesium experiment at room temperature. A substrate with well-controlled disorder has been obtained by photolithographic techniques; using water and a water-glycerol mixture, we have studied the motion of the CL. In this article, we report on the results of this experiment. Quite surprisingly, it turns out that we still find a roughness exponent close to 0.5. We have checked that the dynamics is actually overdamped and quasi-static, so that the standard model should be relevant.

2 Experimental setup

A sketch of the experimental setup is shown in Figure 2. The plane substrate is a glass plate with random disorder. This plate is partially dipped into a liquid bath with an angle of 10° with respect to the horizon. In order to avoid the deposition of dust particles, the sample and the liquid bath are placed in a closed transparent box; this box also reduces the liquid evaporation. The plate is removed from the bath with a constant velocity thanks to a translation stage. Thus we impose the average velocity v (or drift velocity) of the CL with respect to the substrate. We worked with values of v ranging from $0.2\,\mu$m/s up to $20\,\mu$m/s.

The substrate is a glass plate ($63 \times 63\,\mathrm{mm}^2$) initially covered with a layer of chromium. By a photolithographic process, chromium is removed except in a $20 \times 20\,\mathrm{mm}^2$ area which contains 10^6 chromium patches which act as

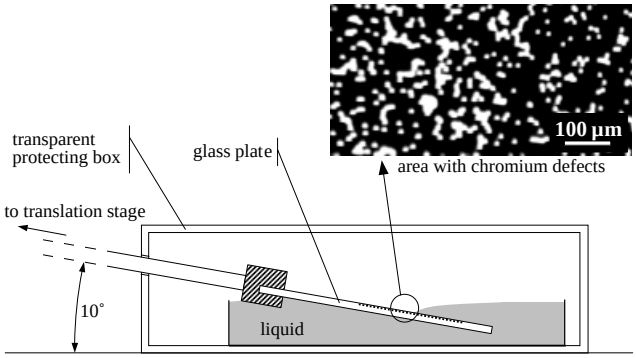

Fig. 2. Sketch of the experimental setup. Inset: photograph of the disordered substrate, the chromium defects appear as white square spots.

Table 1. Table of viscosity and contact angle of the liquids used in our experiments. The accuracy of angle is 2°. On bare chromium, the advancing angle value is roughly 70-80°, receding angle is 40-50°.

		Water	Water/glyc.
Viscosity (Pa · s)		10^{-3}	$20 \cdot 10^{-3}$
contact angle on glass	advancing	58°	53°
	receding	32°	27°
contact angle on disordered substrate	advancing	69°	60°
	receding	40°	36°

defects. These defects have a square shape ($10 \times 10\,\mu\mathrm{m}^2$) and their positions are random (see inset in Fig. 2). This configuration is the same as the one used for the helium experiment, except for the shape of individual defects which were nearly circular in our previous work [11]. As previously, we can safely assume that the correlation in the disorder is short ranged, and the correlation length ξ is $10\,\mu$m. The height of the defects is of the order of 10 nm, much smaller than their lateral size. We have not observed any evidence of pinning on the edge of the defects, so that the defect strength is mainly related to the difference in wettability between glass and chromium (see Tab. 1). The chemicals and procedure used for cleaning the substrate have an influence on the contact angle. In order to obtain reproducible results, the same cleaning procedure is followed before each experiment. The substrate is first rubbed with a soft whipper and rectapure acetone, then with water. Next, the substrate is rinsed with water, dried with nitrogen and kept a few minutes in an oven at about 80 °C. The liquids used in our experiments were water and an aqueous solution of glycerol (70% by weight). These liquids have roughly the same surface tension $\gamma = 70 \times 10^{-3}\,\mathrm{N/m}$. Table 1 shows for those two liquids the viscosity and the advancing and receding contact angles on bare glass and disordered substrate. The angles are measured on images of droplets seen under low-angle incidence. The measurement of contact angle on bare chromium is not possible on our sample. Measures on other samples lead to advancing angle values between 70°

and 80° and receding angle values between 40° and 50° for both liquids.

The CL is observed with a long-working-distance microscope equipped with coaxial illumination and an ordinary progressive-scan CCD camera. A mirror positioned under the substrate allows to enhance the contrast between the image of the dry part of the substrate and the one of the meniscus (Fig. 1). The position of the CL can be located, with an accuracy of one pixel, by applying a threshold to the 8 bit images. Such a simple processing allows real-time image analysis (25 frames per second). The magnification has been varied between $\times 0.7$ and $\times 4$, which yields a resolution in the substrate plane between $10\,\mu$m and $2\,\mu$m. In order to measure the CL dynamics during fast jumps, we have also used a fast CCD camera (500 images per second). In this case, the images have a lower signal-to-noise ratio and a lower resolution. For each pixel column i, the intensity $I(x_i, y)$ is fitted by a hyperbolic tangent function $\tanh((y-y_0)/\delta)$; the location $\eta(x_i)$ of the CL is defined as the inflection point y_0. With this procedure, the final accuracy is 0.5 pixel ($1.3\,\mu$m).

3 The roughness of the contact line

In a typical experiment, the CL sweeps an area of $50\,\mathrm{mm}^2$. The roughness $W(L)$ is averaged over typically 1000 successive configurations of the line, so that the average distance between two configurations is of the order of $10\,\mu$m. The measured roughness $W(L)$ is shown in Figure 3 for different drift velocities and different liquids. Values for $L > 2$ mm are not meaningful because of edge effect. Indeed, the width of the disordered part of the plate is 20 mm, and the edges induce a distortion of the CL whose extension is of the order of the capillary length $L_\mathrm{c} \equiv (\gamma/\rho g)^{1/2}$ (ρ is the liquid density and g the gravitational acceleration). L_c is about 2.5 mm. To avoid edge effect, only the central part of the plate was used; and we have checked that the curvature of the CL averaged over all the configurations is zero. The dispersion between the curves shown in Figure 3 is similar to the dispersion between successive runs in the same experimental condition, so that the overall scatter of the data gives an estimate of the reproducibility and accuracy on $W(L)$. We have done experiments with various magnifications, in order to check that the noise due to the pixel finite size does not lead to an increase of $W(L)$ for small L. Such an effect is negligible as soon as $L > 25\,\mu$m, as shown in Figure 3.

In the experimental range of parameters, the roughness does not depend neither on the drift velocity v nor on the viscosity η. This is not very surprising since the capillary number $Ca \equiv \eta v/\gamma$ is always smaller than 10^{-5}. In such a range of Ca, the viscous dissipation is small compared to the hysteresis. This means that the system is always at the depinning threshold. We have fitted the roughness $W(L)$ by a power law for $2\xi < L < L_\mathrm{c}/2$. For all runs, the roughness exponent is found to lie between 0.48 and 0.54. We checked that the fitted values are not sensitive to the cutoffs 2ξ and $L_\mathrm{c}/2$. We conclude that $\zeta = 0.51 \pm 0.03$. Thus we find a value of the roughness exponent which is significantly larger than the theoretical predictions. Quite unexpectedly, ζ is comparable with the result of our previous work with liquid helium [11].

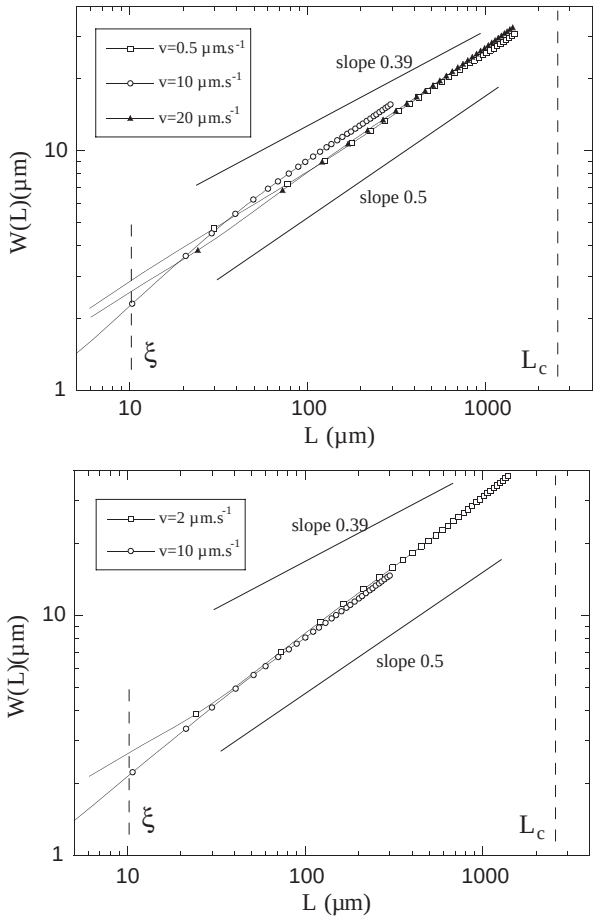

Fig. 3. Roughness W as a function of distance L for different drift velocities. The upper (respectively, lower) graph corresponds to data obtained with water (respectively, water-glycerol mixture). For both graphs, the data ∘ have been obtained with a larger magnification (resolution 2.1 μm) than the others (resolution 6.1 μm).

4 Dynamics of the contact line

4.1 Quasi-static motion

The fact that we find a similar value for ζ for a superfluid as well as for a viscous fluid is rather puzzling, and it was necessary to check the hypothesis that the motion of the CL is quasi-static in water. We have thus performed a study of the dynamics of the CL.

When a low mean velocity v is imposed, the motion of the CL is discontinuous. Most of the time, the CL moves very slowly while remaining pinned on some defects. Sometimes, the CL meets a new defect and jumps forward to a new pinned position. This jump is called an avalanche. Such a dynamics involves a large range of velocities and a fast camera is needed to perform a quantitative study

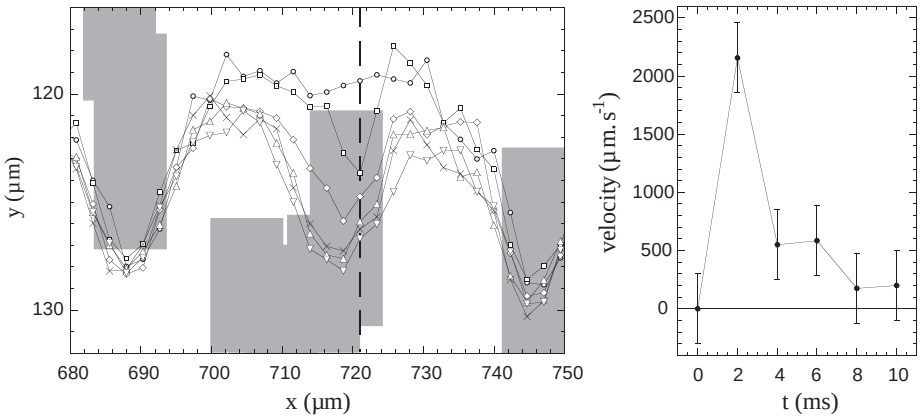

Fig. 4. Left: successive positions of the contact line at the meeting of a defect (defects are shown as grey areas). Right: local velocity at $x = 721\,\mu$m as a function of time. The liquid is a water-glycerol mixture and the drift velocity is $2\,\mu$m/s. The frame rate is 500 Hz and the resolution is $1.3\,\mu$m.

of the motion of the CL. A local jump is shown in Figure 4. In order to increase the accuracy in the position of the chromium defects, these defects are located in a second step with an ordinary CCD camera (the resolution is then 1.3 μm). Their positions are superimposed in gray in Figure 4.

When the CL meets a non-wetting defect of chromium, it is submitted to a pulling force due to the change in the local spreading coefficient. Within two milliseconds, the CL velocity reaches a high value, of the order of 2 or 3 mm/s (Fig. 4). This maximum velocity does neither depend on the drift velocity nor on the viscosity. Then, the local velocity of the CL on the defect decreases to a small value before the liquid has completely uncovered the defect: the acceleration is negative though the local pulling force has not vanished. Thus, inertia may play a role in the first millisecond of the jump but it is not efficient enough to make the CL jump over a defect. For displacements of order ξ, the CL motion can be considered as overdamped. Thus, one can neglect a possible $\partial^2\eta/\partial t^2$ term in the dynamic equation, as assumed when writing equation (1).

The inertia can have another indirect effect on the dynamics of the CL, because of its non-local elasticity. When writing the elastic restoring force on the CL (Eq. (2)), one assumes that the shape of the whole meniscus follows instantaneously the local distortions of the CL. This was shown to be false for superfluid helium. In order to find out what is the situation for usual liquids, we have studied longer sequences, such as the one shown in Figure 5, whose duration is about two seconds. During this sequence, the drift velocity is $2\,\mu$m/s. The lower part of Figure 5 shows the temporal evolution of the positions $y(x_i, t)$ of the CL for some fixed values x_i of x. These values are represented in the upper part of Figure 5 by verticals gray lines. On this example, before $t = 1088$ ms, the motion of the CL is slow ($\simeq 1\,\mu$m/s for $i = 6$). This slow motion corresponds to a pinned configuration since the CL goes through a fixed set of defects. A first event occurs at $t = 1088$ ms on two defects ($x = 560\,\mu$m and $x = 610\,\mu$m). The deformation of the CL due to a meeting with a defect modifies the elastic restoring force. The local velocity of the

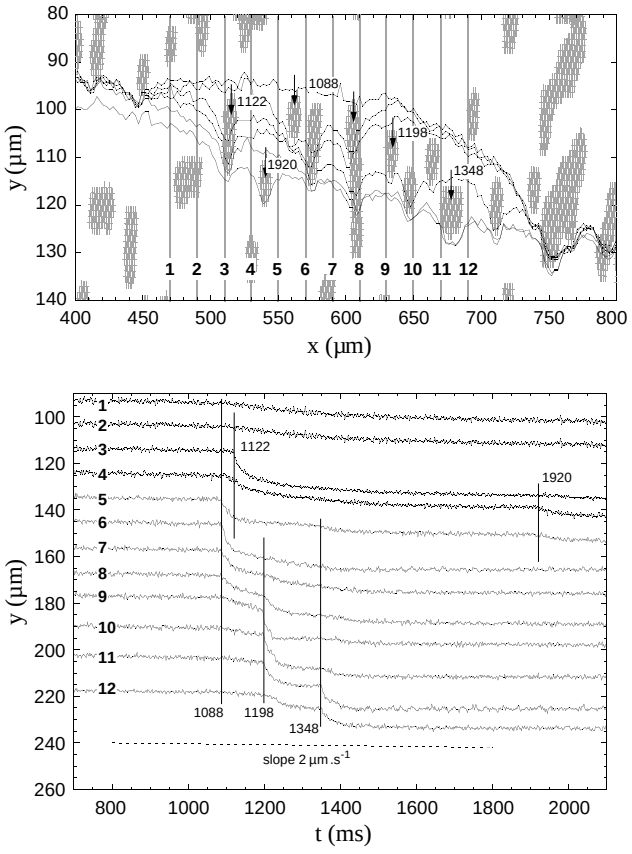

Fig. 5. Upper part: positions of the contact line just before the meeting of a new defect. The gray patterns represent roughly the defects. The arrows show the defects met by the CL and the meeting time in ms. At $t = 1088$ ms, the CL meets simultaneously two defects ($x \simeq 560\,\mu$m and $x \simeq 605\,\mu$m). Note the difference between the horizontal and vertical scales. Lower part: temporal evolution of the position $\eta(x_i, t)$ of the CL for fixed values $x_1 ... x_{12}$ of x. The x_i values are shown by vertical lines in the upper part. For a better readability, the curves $\eta(x_i, t)$ are arbitrarily translated along the y-axis. Vertical lines are placed at times of meeting between the CL and the defects. The dashed line represents the actual drift velocity $v = 2\,\mu$m/s.

CL increases suddenly in the vicinity of the defect: one observes cusps in the $y(x_i, t)$ curves in the lower part of Figure 5. These cusps appear *simultaneously* (more precisely, within one time step). Actually, the meniscus deformation which triggers the CL acceleration propagates at a finite velocity. The relevant velocity is the velocity of surface waves c. For a liquid depth of 1 mm and for a wavelength of 100 μm, the usual dispersion relation for surface waves yields $c \sim 2$ m/s. Such a high velocity cannot be measured with our setup: the deformation propagates over one millimeter in one time step, so that all points of the CL seem to accelerate simultaneously. Still, the experiment shows that the meniscus shape relaxes much faster than the CL. As a consequence, one can safely forget any retardation effect in the elastic restoring force despite the long-range nature of the CL elasticity and equation (2) is expected to be valid.

The assumption of a quasi-static motion of the CL is thus valid for the experiments with ordinary liquids. This is a fundamental difference with our previous experiments with liquid helium [11]. For helium, we have proposed that the inertia plays an important role in the dynamics: as the lateral propagation of an avalanche occurs at the same velocity as the propagation of capillary waves, it is likely that dynamic stress overshoots exist, as proposed by Schwartz and Fisher [12].

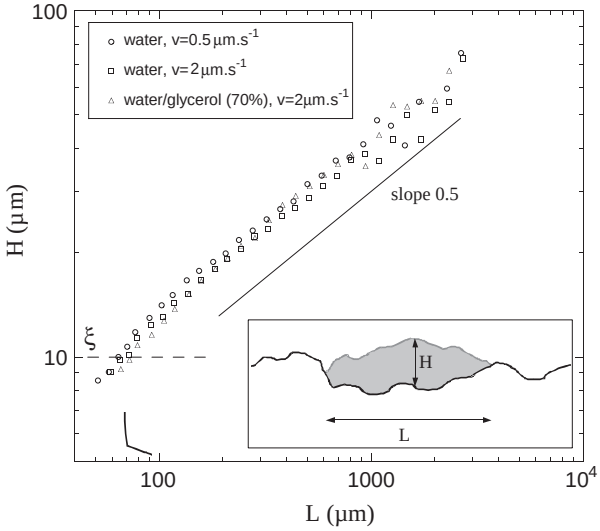

Fig. 6. Average height H of an avalanche of length L for different drift velocities and different viscosities. One finds that H scales roughly like $L^{0.5}$, which is consistent with the value of the roughness exponent ζ. Inset: schematic representation of an avalanche.

4.2 Avalanches

In order to characterize the dynamics of the contact line, we have studied the properties of the avalanches. One first needs a criterion for defining the beginning and the end of an avalanche. An avalanche always starts by a fast jump, such as the event at $t = 1088$ ms in Figure 5. An initial event can trigger secondary jumps, such as the ones at $t = 1122$ ms and $t = 1198$ ms. Deciding where the avalanche does stop is not always easy: is the fourth event at $t = 1348$ ms a direct consequence of the three others? A reasonable criterion is to consider a line configuration as pinned if its velocity is everywhere smaller than the drift velocity. With this criterion, the event at $t = 1348$ ms belongs to the same avalanche as the three others. Finally, this particular avalanche has a length L along x of the order of 300 μm and a height H along y of the order of 25 μm.

Carrying out systematically such a procedure is impossible because of the sequence duration that cannot exceed four seconds with the fast camera. In order to get enough statistics, we need to use a standard camera with an acquisition time $t_{\rm acq} = 40$ ms. We consider that a line is in a pinned configuration if its position in two successive images is not changed by more than three successive pixels. An avalanche is defined as the swept area delimited by two successive pinned positions of the CL, which is characterized by its length L and its height H (see inset in Fig. 6). By changing the magnification, we have checked that the results are not sensitive to the threshold of three pixels. By changing $t_{\rm acq}$, we have also checked that $t_{\rm acq}$ is small enough not to lump together two distinct avalanches, at least for drift velocities smaller than 2 μm/s. Still, there is an additional difficulty due to the non-local nature of the elastic interaction: *a priori*, simultaneous depinning events are parts of a single avalanche, even if the depinning regions of the CL are disconnected. We have studied carefully a number of fast sequences. It turns out that, when the CL jumps on a defect, its velocity is increased only in a rather small region around the defect (see Fig. 5), typically 100 μm. Thus, we consider simultaneous disconnected jumps as non-correlated avalanches.

As a first result, we have found that the CL goes through almost the same configurations for different runs. Thus the motion is deterministic, which ensures that the thermal noise is negligible for such macroscopic defects. The absence of dependence in v is a further evidence that the system is close to the depinning threshold.

Figure 6 shows H as a function of L. Only avalanches containing at least one defect, *i.e.* with $H > \xi$, are represented. The aspect ratio of the avalanches depends neither on drift velocity nor on viscosity of the liquid. One expects that the scaling of $H(L)$ is the same as the one of the roughness $W(L)$. Indeed, for $h > \xi = 10\,\mu$m, $H(L)$ scales as a power law with an exponent of 0.51 ± 0.03, which is the same value as the one of the roughness exponent ζ.

The distribution in size of the avalanches is shown in Figure 7. The probability $P(L)$ of occurrence of an avalanche is plotted as a function of its length L. This probability is obtained by counting the number $N(L)$ of avalanches for each value of L. This number is normalized first by the effective area $A_{\rm tot}$ swept by the CL during the experiment, which is equal to the total advance of the CL ($v\times$duration of the experiment) times the effective length of the CL. Let us call $L_{\rm field}$ the size of the acquisition field. The avalanches detected on the edge of the acquisition field are not counted so that the effective length of the CL on which avalanches of width L

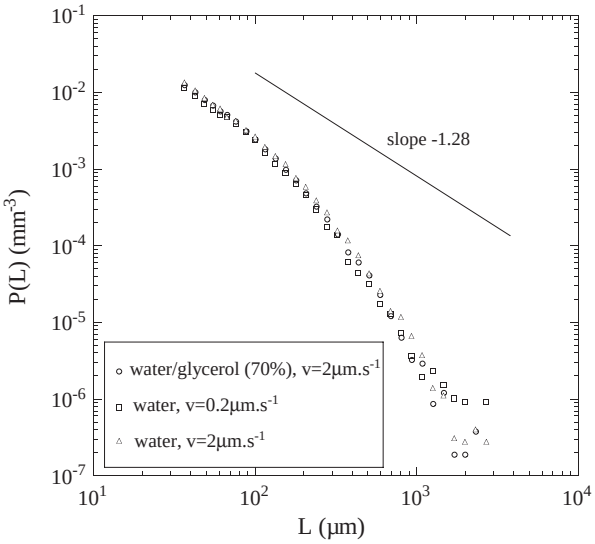

Fig. 7. Probability $P(L)$ of occurrence of an avalanche of length L for different drift velocities and different viscosities. P is the number of avalanches divided by the effective area swept by the CL and by the effective pixel size. This curves are obtained with the same magnification of the microscope; other magnifications lead to the same curves. The solid line is the power law dependence expected from numerical simulation.

are detected is $L_{\rm field} - L$. Finally, in order to compare quantitatively experiments done with various magnification, $P(L)$ is also normalized by the pixel size p in the substrate plane: $P(L) \equiv N(L)/(p\,A_{\rm tot})$. One finds that the size distribution is very reproducible, and depends neither on the drift velocity nor on the viscosity of the liquid. At depinning threshold, one expects this distribution to follow a power law: we have also shown in Figure 7 the scaling law $P(L) \sim L^{-1.28}$ deduced from numerical simulation [10]. Actually, the curve $P(L)$ is found to decrease faster than a power law. This is different from the helium case, where the $P(L)$ was found to decrease rather more slowly than predicted. This difference between the two systems is consistent with the idea that inertia promotes larger avalanches.

5 Discussion

In contrast with the helium experiment, the viscous liquids used in the present experiment lead to an ordinary overdamped motion of the contact line. Thus, most assumptions leading to equation (1) seem to be valid: quasistatic motion and no thermal noise. However, we still find a value of ζ which is larger than predicted; the size distribution of avalanches is also unexpected. Let us propose two possible explanations for this discrepancy.

First, it has been shown by Rosso and Krauth that small non-harmonic correction to the elastic energy can lead to a strong change in the roughness exponent [15]. Since their work is restricted to short-range elastic interactions, it is not possible to conclude how ζ would be modified for long-range elasticity. Moreover, in the case of the CL the first correction to the dominant quadratic term is not a fourth-order term, but a third-order term in the CL displacement [16].

Second, it is assumed in equation (1) that the dissipative term is linear in velocity. Physically, this corresponds to a viscous dissipation due to the shear flow in the wedge close to the contact line [4]. The dissipation coefficient μ is then proportional to the viscosity, and is a complicated function of the contact angle [17]. In our experiment, the maximal local velocity during a jump does not depend on viscosity. This is an indication that one cannot account for the dissipation by a simple shear flow in the wedge [18]. In our range of velocities and contact angle, it is more likely that the CL dynamics should be described in terms of activated molecular jumps at the CL [18]. In such a molecular-kinetic model, one expects the velocity to be a highly non-linear function of the applied force F. This has been checked in a number of experiments [18,19]. In the present experiment, such a model is presumably relevant: the hysteresis on homogeneous glass (or chromium) substrate shows clearly that there exists some microscopic disorder at a scale much smaller than ξ. Moreover, the local CL dynamics involves a wide range of velocities. Thus, it is possible that a strongly non-linear $v(F)$-dependence changes the dynamics of the system, even at the depinning threshold.

Further experimental work is needed to get a better understanding of the CL behaviour. Studying precisely more simple problems like the pinning on a single defect could help to understand the effect of a non-linear dissipative term. It would also be interesting to investigate the dynamics of the system for higher drift velocities, closer to the maximum local velocity in the jumps.

References

1. K. Dahmen, J.P. Sethna, Phys. Rev. B **53**, 14872 (1996).
2. O. Narayan, D.S. Fischer, Phys. Rev. B **46**, 11520 (1992).
3. D. Ertas, M. Kardar, Phys. Rev. E **49**, 2532(R) (1994).
4. J.F. Joanny, P.G. de Gennes, J. Chem. Phys. **81**, 552 (1984).
5. A. Hazareezing, M. Mézard, Phys. Rev. E **60**, 1269 (1999).
6. E. Rolley, C. Guthmann, R. Gombrowicz, V. Repain, Phys. Rev. Lett. **80**, 2865 (1998).
7. P. Chauve, P. Le Doussal, K.J. Wiese, Phys. Rev. Lett. **86**, 1785 (2001).
8. A. Rosso, W. Krauth, Phys. Rev. E **65**, 025101(R) (2002).
9. A. Tanguy, M. Gounelle, S. Roux, Phys. Rev. E **58**, 1577 (1998).
10. Y. Zhou, PhD Thesis, John Hopkins University, Baltimore, 1999.
11. A. Prevost, E. Rolley, C. Guthmann, Phys. Rev. B **65**, 064517 (2002).
12. J.M. Schwartz, D.S. Fischer, Phys. Rev. Lett. **87**, 096107 (2001).
13. J.-M. Di Meglio, Europhys. Lett. **17**, 607 (1992).
14. E.L. Decker, S. Garoff, Langmuir **12**, 2100 (1996); **13**, 6321 (1997).
15. A. Rosso, W. Krauth, Phys. Rev. Lett **87**, 187002 (2001).
16. R. Golestanian, E. Raphaël, private communication.

17. R.G. Cox, J. Fluid Mech. **168**, 169 (1986). Strictly speaking, if μ is θ-dependent, the $v(F)$ characteristic is non-linear. However, as the range in θ is small in our experiment, this non-linearity is not relevant.
18. T.D. Blake, in *Wettability*, edited by J.C. Berg (Marcel Dekker, New York, 1993).
19. A. Prevost, E. Rolley, C. Guthmann, Phys. Rev. Lett. **83**, 348 (1999).